Strong, Tough, Stretchable, and Self-Adhesive Hydrogels from Intrinsically Unstructured Proteins

Mark A. Gonzalez, Joseph R. Simon, Ali Ghoorchian, Zachary Scholl, Shaoting Lin, Michael Rubinstein, Piotr Marszalek, Ashutosh Chilkoti, Gabriel P. López, and Xuanhe Zhao**

Modern techniques in molecular biology provide exquisite molecular-level control over engineered proteins and have enabled the design of recombinant protein-based hydrogels for diverse applications such as scaffolds for tissue regeneration and drug delivery, coatings for medical devices, and actuators for optical and microfluidic devices.[1–3] Because the performance of protein-based materials is often severely limited by their mechanical behaviors, intense effort has been devoted to designing protein networks with extraordinary mechanical properties, such as extremely high strength, toughness and stretchability, insensitivity to structural defects, and the capacity for self-healing.[4–9] The strategies employed thus far to achieve these properties are primarily focused on incorporating structured protein domains, such as coiled coils, titin-like motifs, and folded fibrin.[6,10–12] The interactions between, and/or unfolding of, these structured domains dissipate mechanical energy and maintain high elasticity of protein networks to enhance the strength and toughness of the resultant material.[13] Despite these successes, the synthesis of hydrogels containing highly structured proteins is limited by the often relatively low and variable production yield. Additionally, many of these proteins can elicit unwanted biological responses due to their tertiary structure, ultimately limiting material functionality, and use in target applications. Conversely, unstructured proteins (i.e., without tertiary structure) are relatively simple to design, can be easily synthesized with high yield, and can be biologically inert;[14] however, previously reported materials based on unstructured proteins have not demonstrated the levels of strength, toughness, and stretchability enabled by structured domains.[6,10–12,15] How to achieve extraordinary mechanical properties in hydrogels fully comprised of unstructured proteins remains a fundamental question in the field of protein-based materials.

To investigate this, we developed hydrogels comprised of designer unstructured proteins. We chose elastin-like polypeptides (ELPs) as a model protein system for the following reasons: (i) they are unstructured and exhibit controllable solubility in water;[16] (ii) they can be expressed in bacterial expression systems and easily purified in high yield, which is critical to obtaining gram-scale quantities required to fabricate bulk hydrogels;[17] (iii) they show high tolerance to the periodic incorporation of other non-ELP peptide motifs;[18] and (iv) they are nontoxic and biocompatible.[19] Using plasmid reconstruction by recursive directional ligation, a method that enables assembly of gene segments in a modular and programmable fashion (Figure S1, Supporting Information), we synthesized three genes encoding for proteins that consist of ELP domains interspersed with periodic repeats of two different types of crosslinking domains, as shown in **Figure 1**A.[2] This gene assembly method enables us to precisely control the composition, length, and density of each domain, which together with the overall molecular weight of the protein, are important for controlling the mechanical properties of materials made of these proteins. The metal crosslinkable proteins (MCPs) contain eight elastin-like domains comprised of five (MCP1) or ten (MCP2) ELP pentapeptides, each separated by a zinc-binding

M. A. Gonzalez, Prof. P. Marszalek, Prof. X. Zhao
NSF Research Triangle Materials Research Science and Engineering Center
Department of Mechanical Engineering
Duke University
Durham, NC 27708, USA
E-mail: zhaox@mit.edu

J. R. Simon, Dr. A. Ghoorchian, Prof. A. Chilkoti, Prof. G. P. López
NSF Research Triangle Materials Research Science and Engineering Center
Department of Biomedical Engineering
Duke University
Durham, NC 27708, USA
E-mail: gplopez@unm.edu

Z. Scholl
Department of Mechanical Engineering
Duke University
Durham, NC 27708, USA

S. Lin, Prof. X. Zhao
Soft Active Materials Laboratory
Department of Mechanical Engineering
Massachusetts Institute of Technology
Cambridge, MA 02139, USA

Prof. M. Rubinstein
NSF Research Triangle Materials Research Science and Engineering Center
Department of Chemistry
University of North Carolina at Chapel Hill
Chapel Hill, NC 27599, USA

Prof. G. P. López
Department of Chemical and Biological Engineering
The University of New Mexico
Albuquerque, NM 87131, USA

Prof. X. Zhao
Department of Civil Engineering
Massachusetts Institute of Technology
Cambridge, MA 02139, USA

DOI: 10.1002/adma.201604743

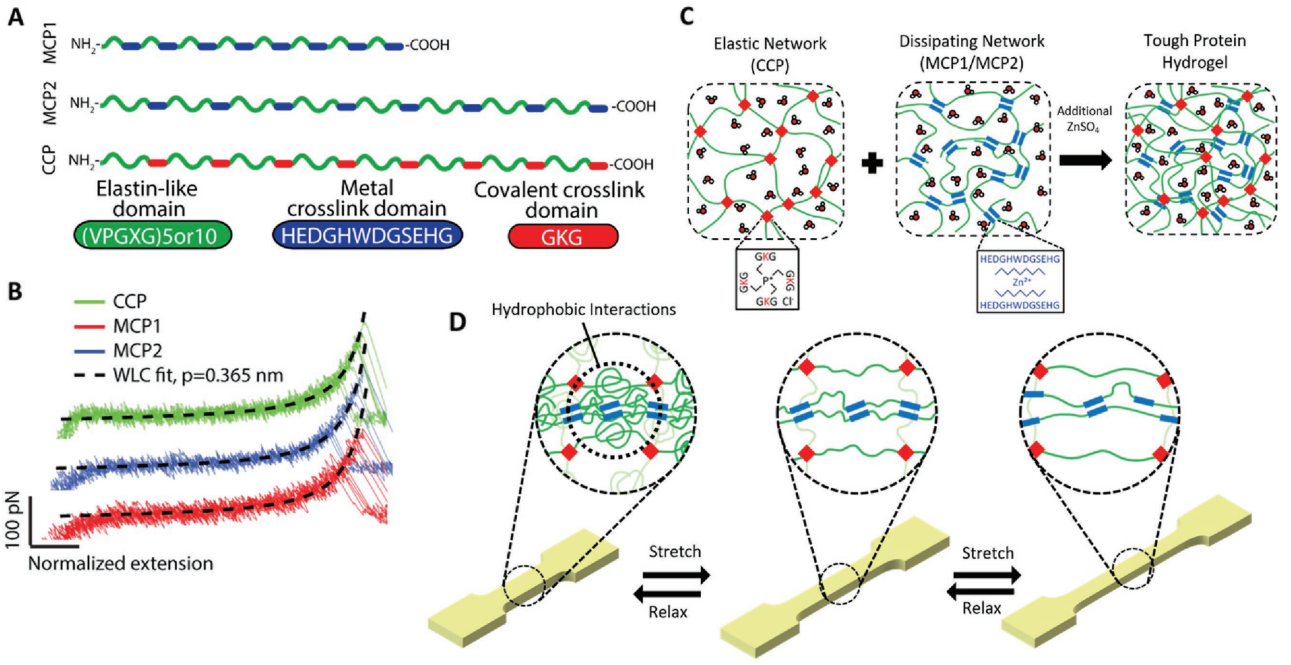

Figure 1. Design of hydrogels with hybrid crosslinking based on unstructured proteins. A) Schematic representation of designer unstructured proteins capable of covalent (CCP) and metal coordination (MCP 1 and 2) crosslinking. Elastin-like polypeptide domains (green) of varying length are interspersed with metal crosslinkable (blue) or covalently crosslinkable (red) domains. B) Force-extension profiles of individual molecules show similar elasticity. Each molecule follows the worm-like chain model for an unfolded polypeptide with a persistence of 0.365 nm, which is indicative of an unstructured polypeptide. C) Schematic illustrations of the covalently crosslinked networks, metal crosslinked networks, and interpenetrating networks (water molecules not to scale). Tough hydrogels are formed, depending on the concentration of $ZnSO_4$ present in the system. D) When the interpenetrating network hydrogel is stretched and relaxed, the phase transitioned ELP can be disrupted and reformed, respectively. Reversible decrosslinking/crosslinking also occurs within the MCP network while the CCP network maintains elasticity throughout.

motif found in matrix metalloproteinases (Figure 1A).[20] The zinc-binding motif we chose has the amino acid sequence HEDGHWDGSEHGY, which we have previously shown to efficiently bind Zn^{2+} and form stiff hydrogels when displayed on the coronae of micelles in the presence of $ZnSO_4$.[21] While many transition metal-binding peptide sequences exist, we chose one that specifically chelates Zn^{2+} because Zn^{2+} is significantly less toxic than Ni^{2+} and Cu^{2+}.[22,23] The covalently crosslinkable protein (CCP) contains the same eight elastin-like domains comprised of ten ELP pentapeptides separated by the peptide, GKG (Glycine-Lysine-Glycine), (Figure 1A) wherein the lysine (K) residue in the tripeptide serves as a covalent crosslinking site.[21] Each of these proteins was expressed and purified in high yield (≈350 mg L^{-1} bacterial culture) using the inverse transition cycling purification method (Figure S1, Supporting Information).[24] These techniques enable the synthesis of gram-scale quantities of proteins with >97% purity as illustrated in Figure S2 (Supporting Information). To validate that the CCP, MCP1, and MCP2 do not contain structured domains, we measured their resistance to force using single-molecule force-spectroscopy (Materials and Methods, Figure S3, Supporting Information). Unstructured proteins have a mechanical resistance that very closely follows a worm-like chain model of elasticity with a persistence length of ≈0.4 nm (which is close to the length of a peptide bond), while structured molecules exhibit significant deviations from a worm-like chain model or show large hysteresis between extension and retraction curves due to work dissipated from unfolding protein structures.[25,26] Force-extension curves of single molecules of CCP, MCP1, and MCP2 show that these molecules indeed closely follow a worm-like chain model of elasticity (Figure 1B) and show completely reversible behavior absent of hysteresis (Figure S4, Supporting Information)—indicating that they are unstructured proteins. The unstructured nature of the proteins was also confirmed by circular dichroism spectroscopy in which CCP, MCP1, and MCP2 show characteristics of disordered polypeptides (Figure S5, Supporting Information).[27]

After expressing and purifying the proteins, we formed networks by crosslinking them with small molecules and metal ions (Figure S6, Supporting Information). In brief, CCP and MCP1 or MCP2 were resuspended in a buffered solution and subsequently combined at various concentrations to form a solution containing a mixture of proteins. Tetrakis(hydroxymethyl)phosphonium chloride (THPC) was then added to the mixture to covalently crosslink the CCP networks.[28] The resultant hydrogels contain 70–75 wt% water and appear transparent at room temperature (**Figure 2**B). The hydrogels were then immersed in zinc sulfate solutions of different concentrations to crosslink the MCP1 or MCP2 proteins via metal coordination. The water content in the resultant networks ranges from 32 to 96 wt%, dependent on the constituent proteins and concentrations of Zn^{2+} in the solutions (Figure 2A). Unless otherwise noted, herein the reported water content and protein concentrations represent the values within the hydrogel prior to exposure to metal ions. The networks containing a concentration of 2.0×10^{-3} M or higher $ZnSO_4$ appear

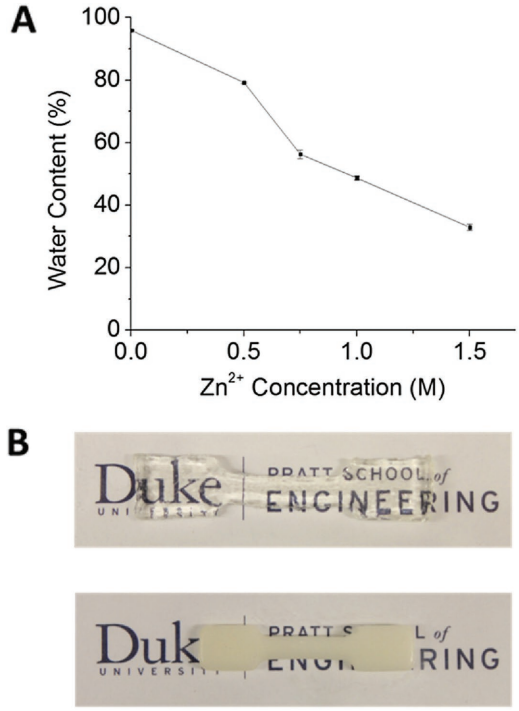

Figure 2. Water content of ELP-based networks. A) Water content percentage versus concentration of Zn^{2+} within the hydrogel ($N = 3$). The hydrogels initially contain 20 wt% CCP and 5 wt% MCP1 after covalent crosslinking. Decrease in water content is associated with decreased solvent quality due to increase of salt concentration. (Note: Error bars for all data are less than 1% and are smaller than the data point symbols.) B) Photos of a hydrogel (top) transitioning into an opaque hydrogel (bottom) after submersion in a 1.5 M Zn^{2+} bath. The covalently crosslinked network contained 20 wt% CCP and 5 wt% MCP1. Transition occurs at 2×10^{-3} M Zn^{2+} concentrations (refer to Figure S13, Supporting Information).

opaque at room temperature (Figure 2B and Figure S13, Supporting Information) due to the effect of the kosmotropic salt lowering the cloud point of the aqueous ELP to a temperature below ambient.[29]

By simply controlling the concentrations of the proteins (CCP, MCP1, and MCP2) and the crosslinkers (THPC and Zn^{2+}), it is possible to synthesize extremely strong, tough, stretchable, and self-adhesive hydrogels (**Figure 3**A,B). As a control, we found that a crosslinked network containing only CCP (no MCP1/2 nor $ZnSO_4$) results in a hydrogel that can sustain uniaxial strain no more than 39% at room temperature (Figure 3C and see Figure S9, Supporting Information, for details of the mechanical tests). Hydrogels containing a lower concentration of crosslinked CCP and either MCP1 or MCP2, in the absence of $ZnSO_4$, demonstrated improved stretchability over the above control (average uniaxial strain of 94% and 72%, respectively) at the cost of reducing the ultimate strength by approximately an order of magnitude. The introduction of $ZnSO_4$ at a threshold concentration of 2×10^{-3} M causes coacervation (i.e., salt induced hydrophobic collapse) of all three ELP hydrogels, introducing hydrophobic interactions into the hydrogels.[7] Consequently, addition of 2×10^{-3} M $ZnSO_4$ to the CCP-only hydrogel results in a subtle increase in stretchability above the control (Figure 3C). Conversely, addition of 2×10^{-3} M $ZnSO_4$ to CCP/MCP1 and CCP/MCP2 hydrogels results in significant improvements in stretchability (Figure 3C), suggesting metal-coordination complexes have formed within the network and are contributing to the change in mechanical behavior in addition to the hydrophobic–hydrophobic interactions.

To further enhance the mechanical properties of these networks, we explored higher salt concentrations. At concentrations of 1.5 M $ZnSO_4$, we observe multiple orders of magnitude improvements of stiffness, stretchability, and ultimate strength compared with hydrogels containing 2×10^{-3} M $ZnSO_4$ or less. The enhancement of mechanical properties is more pronounced in CCP/MCP1 and CCP/MCP2 than in CCP-alone, potentially due to the combined effects of metal coordination and hydrophobic interactions within CCP/MCP1 and CCP/MCP2 networks (Figure 3C).[30] For example, a hydrogel with 20 wt% CCP and 5 wt% MCP1 crosslinked by 10.8×10^{-3} M THPC and 1.5 M Zn^{2+} can achieve an average tensile strength of 2.6 MPa at an average uniaxial strain of 549%. As demonstrated in Figure 3B, a segment of our hydrogel with a 40 mm^2 cross-sectional area can easily hold a weight of 0.5 kg.

The design of tough materials generally relies on implementing mechanisms to dissipate mechanical energy and maintain high elasticity.[13,31] In this study, the CCP network enables high elasticity, while the dissipation of mechanical energy results from the reversible crosslinks from metal coordination and hydrophobic interactions (Figure 1C)—a mechanism that is distinct from the unfolding of structured domains utilized in many previous studies of protein hydrogels.[8] A material's dissipative properties can be characterized by the hysteresis loop in its stress–strain curve (i.e., Figure 3D,E), where the area of the loop gives the mechanical energy dissipated per volume of the material in one loading–unloading cycle.[32] From Figure 3D, it is evident that a 25 wt% CCP network without MCP yields a negligible hysteresis loop (see Figure S8, Supporting Information, for additional details regarding CCP hysteresis). The hysteresis loop can be increased by crosslinking 5 wt% of MCP2 interpenetrated with 20 wt% of CCP in 1 M Zn^{2+}. Replacing the MCP2 with the same mass of MCP1 can further enhance the dissipation, as indicated by the larger hysteresis loop in Figure 3D, presumably due to the higher densities of reversible crosslinking sites in MCP1 than MCP2 (Figure 1A).

Changing the concentration of Zn^{2+} ions within the networks enables control over their dissipative properties. As shown in Figure 3E, the hysteresis loop for a hydrogel with 5 wt% MCP2 and 20 wt% CCP only becomes pronounced at Zn^{2+} concentrations of 1.0 M and greater, indicating that hydrophobic interactions contribute significantly to the dissipative properties of CCP/MCP2 networks. In addition, as shown in Figure 3F, the hysteresis loops in stress–strain curves of a CCP/MCP1 hydrogel can be recovered over various time intervals (i.e., 0–15 min) after one loading–unloading cycle, indicating the ability of the gel to retain its initial mechanical strength after many loading cycles. This recoverable dissipative property is critical to the design of antifatigue hydrogels that can maintain high toughness over multiple cycles of loading and unloading.[30]

We further used pure-shear tests to measure the fracture toughness of the materials designed with different dissipative properties (Figure S10, Supporting Information). We fixed the

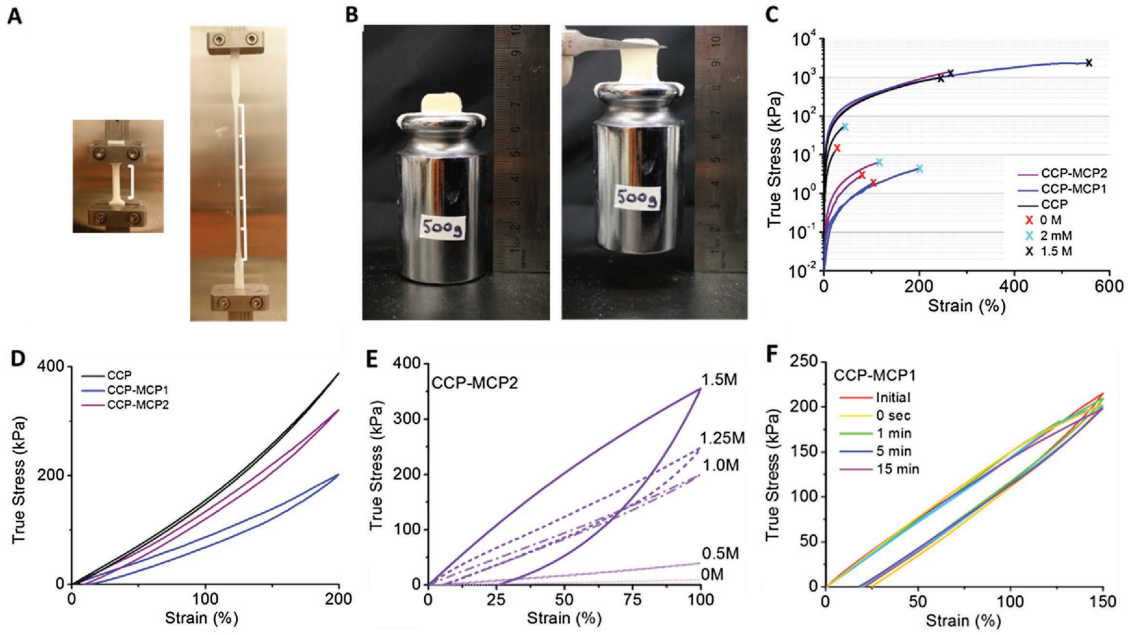

Figure 3. Hydrogels comprised of unstructured proteins exhibit extraordinary mechanical properties. A) A hydrogel with 20 wt% CCP and 5 wt% MCP1 soaked in 1.5 M Zn^{2+} can be stretched over five times its original length under uniaxial tension. B) The same hydrogel with a cross-section area of 40 mm^2 can support a weight of 0.5 kg. C) Stress versus strain curves of hydrogel samples containing 25 wt% CCP (black), 20 wt% CCP + 5 wt% MCP1 (blue), and 20 wt% CCP + 5 wt% MCP2 (purple) under uniaxial tension to failure. The average tensile strength of the strongest dual network hydrogel reaches 2.4 MPa. See Figure S7 (Supporting Information) for additional data sets. D) Stress versus strain curves of hydrogels with 25 wt% CCP (red), 20 wt% CCP and 5 wt% MCP1 (blue), and 20 wt% CCP and 5 wt% MCP2 (purple) soaked in 1.0 M Zn^{2+} under uniaxial tension and relaxation. The stress–strain hysteresis loop and strength varies primarily with the strength of the ELP's hydrophobic interactions within the dual network system. E) Stress versus strain curves with 20 wt% CCP and 5 wt% MCP2 networks soaked in different concentrations of Zn^{2+} under uniaxial tension and relaxation. The stress–strain hysteresis loop varies with the concentration of Zn^{2+}. F) Stress versus strain curves of gels with 20 wt% CCP and 5 wt% MCP1 soaked in 1.0 M Zn^{2+} under uniaxial tension/relaxation cycles at varying intervals between testing. The stress–strain hysteresis loop is recovered after every loading–unloading cycle.

concentrations of pure CCP samples to be 25 wt% and CCP/MCP1 or CCP/MCP2 samples to be 20 and 5 wt%, respectively; these were then immersed in solutions with different concentrations of Zn^{2+} (**Figure 4**). In the absence of metal coordination and phase separation (i.e., 0 M Zn^{2+}), we observed relatively low fracture toughness of 10–30 J m^{-2} for CCP, CCP/MCP1, and CCP/MCP2 hydrogels, which is comparable to the fracture toughness of common hydrogels (Figure 4A).[13] As we increase the Zn^{2+} concentration, the modulus of all networks increases (Figure 4B), while the fracture toughness also dramatically increases by orders of magnitude, due to mechanical dissipation enabled by reversible crosslinking and hydrophobic interactions. This is contrary to the trend of modulus-toughness tradeoff observed for common hydrogels because the modulus increase in our networks is due to the implementation of multiple dissipating mechanisms.[13] The enhancement of the fracture toughness of CCP/MCP1 is particularly pronounced, from 26 J m^{-2} with 0 M Zn^{2+} to 1330 J m^{-2} with 1.5 M Zn^{2+} (Figure 4A). The higher toughness of CCP/MCP1 compared to CCP/MCP2 at higher concentrations of Zn^{2+} may be due to the higher density of metal crosslinkable sites in CCP/MCP1 leading to better dissipative capability at higher strains. To validate that the CCP/MCP1 hydrogel with 1.5 M Zn^{2+} displays tough characteristics, we further used digital image correlation to measure the strain and stress distribution around an intentionally introduced crack defect (Figure S11, Supporting Information). As shown in Figure 4C, a crack in the hydrogel becomes highly blunted and the principal stress at the crack tip before crack propagation can indeed reach the tensile strength of the same hydrogel (without a notch) under pure-shear tension (Figure 4D), indicating the CCP-MCP1 hydrogel with 1.5 M Zn^{2+} is a tough soft material.[33]

The unstructured protein networks are also self-adhesive. To demonstrate self-adhesion, we performed lap-shear tests on networks containing 20 wt% CCP and 5 wt% MCP2. The CCP/MCP2 network was initially formed and cut into two identical pieces, subsequently reattached together by applying a gentle pressure, and finally immersed in solutions containing different concentrations of Zn^{2+}. From **Figure 5**A, it can be seen that the networks indeed adhere to one other after soaking in Zn^{2+} solutions for a minimum of 60 min. Lap-shear tests were then conducted to quantitatively determine the adhesion strength (i.e., failure force per unit width of the sample, see Figure S12, Supporting Information) between the samples. We observed that the samples adhered in Zn^{2+} solutions (0.5 M and higher) can be highly stretched to strains over 70% before peeling off from each other (Figure 4A,B). In addition, the adhesion strength increases dramatically from 4.37 to 172 N m^{-1} when the concentration of Zn^{2+} is increased from 0 to 1.5 M, indicating that the metal coordination and hydrophobic interactions of the network across the material's interface endows these networks with self-adhesive properties. It is notable that

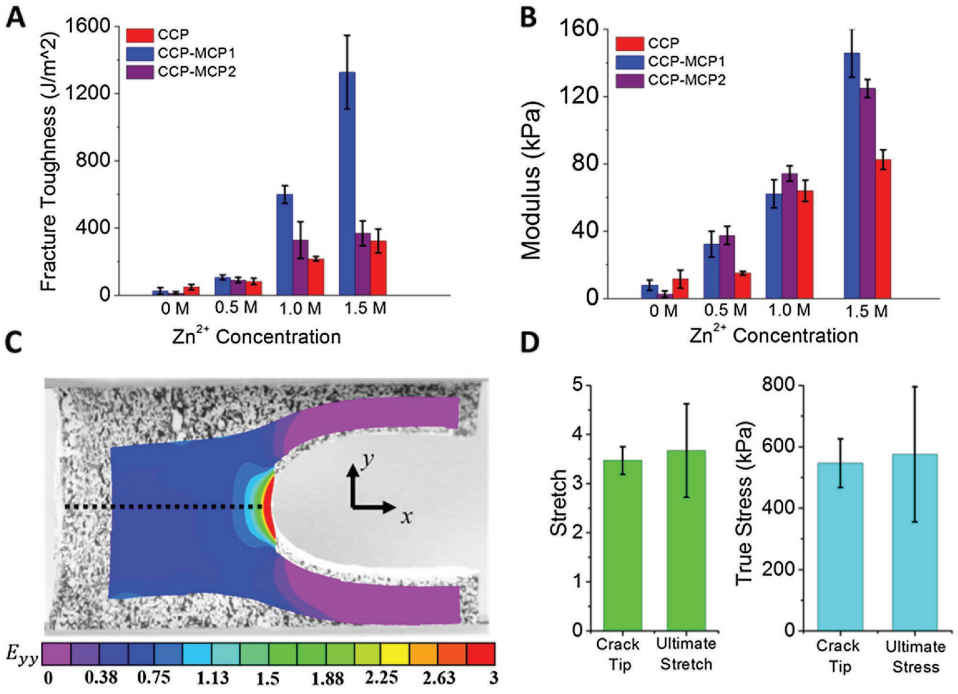

Figure 4. Enhancing modulus and fracture toughness of the hydrogels with multiple dissipating mechanisms. A) Fracture toughness and B) Young's moduli of hydrogels with 25 wt% CCP, 20 wt% CCP and 5 wt% MCP2, and 20 wt% CCP and 5 wt% MCP1. C) Distribution of the maximum principal strain in a notched sample under pure-shear test. The hydrogel contained 20 wt% CCP and 5 wt% MCP1 and was soaked in 1.5 M Zn^{2+}. D) Comparison of maximum principal stress and stretch at the crack tip with the ultimate tensile stress and ultimate stretch of an unnotched sample under pure-shear tension. Values represent mean and standard deviation ($N = 3$ for (A) and (B), $N = 10$ for crack tip, $N = 4$ for ultimate stress and strain for (D)).

the level of adhesion strength achieved here is much higher than recently developed nanoparticle adhesives for gels and biological tissues,[34] although it is lower than the adhesion of tough hydrogels on various nonporous solid surfaces recently achieved.[35,36] Further investigation into the relative contributions of the metal coordination and hydrophobic interactions to enhance adhesion will be considered in future studies.

In summary, we have demonstrated that genetically engineered unstructured proteins with covalent and reversible crosslinking (due to metal coordination and hydrophobic interactions) yield hydrogels with extremely high strength (>2.5 MPa), toughness (>1300 J m^{-2}), stretchability (>500%), and self-adhesion in Zn^{2+} solutions. A number of future research directions now become possible in both the fundamental understanding of the physical properties of protein-based materials and their practical applications. While we have used reversible metal coordination and hydrophobic interactions for mechanical-energy dissipation to toughen our networks, other reversible crosslinking mechanisms such as hydrogen bonding and ionic crosslinking can also be precisely designed through genetic encoding of recombinant proteins. Because the molecular structures of the proteins can be precisely controlled, a systematic optimization of various mechanisms for dissipating mechanical energy and maintaining high elasticity, as well as observing the interactions and inherent properties of polypeptides dictated by their sequence (i.e., hydrophobicity) may lead to protein-based materials with further enhanced physical properties. In addition, the strong, tough, stretchable and self-adhesive materials developed here provide a robust scaffold for use in biomedical and other applications. For example, biofunctional domains such as cell adhesion ligands or growth factors can be coupled into the CCP and/or MCP for controlled interaction with cells in a mechanically robust matrix. Functional groups responsive to pH or biomolecular recognition may also be designed into the proteins for robust actuators in diverse applications.

Experimental Section

Materials: pET24+ cloning vector was purchased from Novagen (Madison, WI). Restriction enzymes, ligation enzymes and Antarctic phosphatase were purchased from New England Biolabs (Ipswich, MA). BL21 *E. coli* cells were purchased from Bioline (Taunton, MA). All salts were purchased from Alfa Aesar (Ward Hill, MA). *E. coli* cell cultures were grown in Terrific Broth (TB) media purchased from MO BIO laboratories Inc. (Carlsbad, CA). DNA extraction kit, DNA gel purification kit, and polymerase chain reaction (PCR) purification kits were purchased from Qiagen Inc. (Germantown, MD).

Gene Synthesis: Genes encoding for proteins were constructed using the recursive directional ligation by plasmid reconstruction method (Figure S1, Supporting Information) as previously described.[2] In brief, the authors modified a pET-24+ cloning vector to include endonuclease recognition sites for AcuI, BseRI, and BglI. The authors digested the modified vector with BseRI and ligated the desired ELP or crosslinking monomer into the vector. The monomer was created by annealing together complementary single-stranded DNA chains that encode for the desired amino acid sequence with "sticky end" overhangs. The vector containing the monomer sequence was then digested with (1) AcuI and BglI to create an "A" population and (2) BseRI and BglI to create a "B" population. The two cut vectors were complementary to one another such that when ligated together the monomer sequence is doubled. This

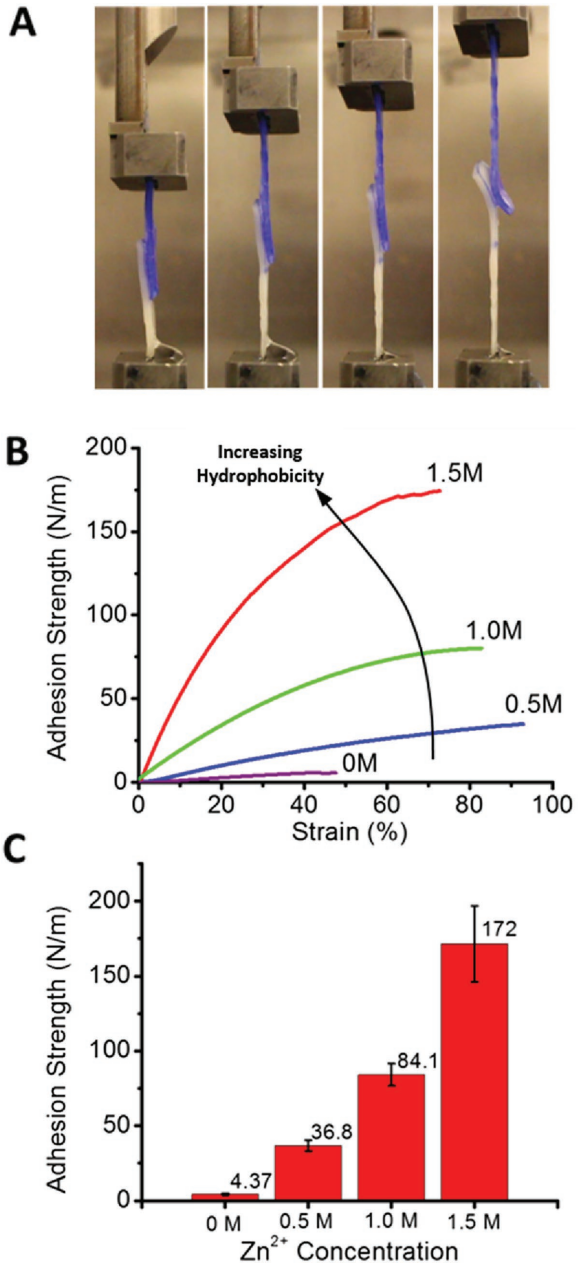

Figure 5. Self-adhesive properties of hydrogels. A) Lap-shear tests of two hydrogel pieces with 20 wt% CCP and 5 wt% MCP2 adhered within a 1.5 M Zn^{2+} solution. One piece of the hydrogel was dyed with 0.1% crystal violet on its surface prior to testing for visualization. The samples can be highly stretched before peeling off from one other. B) Adhesion strength versus strain curves of CCP-MCP2 gels adhered in different concentrations of Zn^{2+}. C) The adhesive strength is shown to increase monotonically with Zn^{2+} concentration, indicating increased adhesion due to hydrophobic interactions at the common interface. Values in (C) represent the mean and standard deviation ($N = 3$).

process was continued until the desired length of protein was achieved. The same procedure applied for insertion of crosslinking domains. The genes encoding for the final sequence of CCP, MCP1, and MCP2 were confirmed by DNA sequencing.

Gene Expression and Protein Purification: The genes encoding for CCP, MCP1, and MCP2 were transformed into chemically competent *Escherichia coli* BL21 cells. The cells were incubated overnight and one colony was used to inoculate a starter culture of sterilized terrific broth media supplemented with kanamycin. The starter culture was shook overnight at 37 °C and 220 rpm. The starter culture was then used to inoculate 6 L of sterilized terrific broth media in 4 L glass flasks, each containing 1 L of media supplemented with 45 μg mL^{-1} of kanamycin. The media was then shaken at 37 °C and 220 rpm for 6–8 h before induction with 0.1×10^{-3} M isopropyl β-D-1-thiogalactopyranoside (IPTG). The cultures were subsequently shaken for 12–14 h at 37 °C and 220 rpm before harvesting and centrifuging at 4 °C and 4000 rpm for 10 min. The resultant cell pellets were used to remove and purify the protein.

The authors purified the protein from the harvested cells by lysing the cells to release the proteins through sonication. The impurities were then removed using the inverse transition cycling method (Figure S1, Supporting Information), described in ref. [37]. This method took advantage of the controlled and reversible phase transition from soluble to insoluble of the elastin-like domain blocks. This was done by cyclic centrifugation steps at high and low temperatures. In most cases, three rounds of centrifugation was sufficient for removing the impurities.

Protein Purity and Molecular Weight Characterization: Protein purity and molecular weight distribution was characterized by 4%–20% gradient tris-glycerol sodium dodecyl sulfate polyacrylamide gel electrophoresis. Protein concentration was determined through lyophilization.

AFM Spectroscopy: All AFM measurements were performed using a custom-built atomic force microscopy (AFM) instrument using MLCT cantilevers (Bruker, Camarillo, CA) which had nominal spring constants of 17 ± 2 pN nm^{-1}.[38] Cantilever spring constants were calibrated in the buffer solution using the energy equipartition theorem.[39] To optimize data collection efficiency and AFM resolution, all measurements were done at a constant velocity of 300 nm s^{-1}, in either PBS pH 7.4 solution or water at room temperature. A sample was prepared by diluting purified protein to 10 μg mL^{-1} and applying 100 μL to a recently evaporated gold slide. The sample was incubated at room temperature for one hour. Then 50 μL was aspirated to remove nonadhering proteins and then AFM measurements were performed. Force-extension curves were recorded during the experiment if they had force >25 pN. These recordings were used for further analysis if the final contour length was greater than 30 nm to eliminate recordings (≈25% of all recordings) that had nonspecific interactions at shorter distances. Approximately 10% of all recordings had multiple force-rupture events, those events did not reveal any reproducible and regular features like force peak magnitude and contour-length increment, and they likely represent recordings obtained on multiple molecules. The majority of all force-extension recordings (≈65% of all recordings) displayed a single rupture event and closely followed the worm-like chain model of polymer elasticity.

Circular Dichroism Spectroscopy: Measurements were performed at 25 °C in pure water with and without zinc ions using an Aviv 62 CD spectrometer equipped with a temperature controller using a 0.1 cm path length quartz cuvette. Protein concentration used was 5×10^{-6} M and wavelength scans for each sample were repeated two times and corrected by subtracting the buffer spectrum. The data were analyzed using Dichroweb online software.

Fabrication of Gel Samples: Gel samples were prepared by combining equal volumes of two separate protein solutions. Lyophilized ELP containing covalent crosslink sites (CCP) was resuspended in phosphate buffered saline (Lonza, without calcium or magnesium) to create a concentration of 40 wt%. Similarly, ELP containing metal crosslink sites (MCP1/MCP2) was also resuspended to create a starting concentration of 10 wt%. THPC (Sigma-Aldrich) was thoroughly mixed into the combined protein solution (0.2 wt%) and poured into the designated mold to covalently crosslink, generally for 12–16 h at room temperature.[40] The cross-linked gel was then removed from the mold and immersed into a predesignated molar concentration of $ZnSO_4$ solution at 4 °C for 12–16 h. Samples were cross-linked at cooler temperatures to both prevent the proteins from phase transitioning

due to the high concentrations of Zn^{2+} before metallic crosslinking was complete and encourage the formation of a homogenous hydrogel. All samples were brought to room temperature prior to all mechanical testing.

Hydrogel Water Content: Fully cross-linked hydrogel samples were weighed at maximum hydration and measured after lyophilization to determine maximum water content after metal crosslinking.

Mechanical Testing: Mechanical tensile testing for dogbone, pure shear, and lap-shear samples was conducted using the TA Instruments RSA III Micro-Strain Analyzer. Samples were tested at room temperature (≈22 °C) at a strain rate of 2% per second. Force–displacement data were collected and processed through TA Orchestrator to generate the stress–strain data shown in Figures 3 and 4.

Lap-Shear Sample Preparation and Testing: Covalently cross-linked rectangular hydrogel samples containing 20% CCP and 5% MCP2 were cut to prepare two identical halves. The halves were partially overlapped and submerged within a Zn^{2+} bath of specified concentration to crosslink overnight at 4 °C. The overlapped samples were pressed together between microscope slides to ensure the two halves completely adhered across the overlapped area uniformly. To prevent the introduction of bending forces to the sample, a spacer was used at the top clamping site to keep each segment of the sample parallel to the tensile direction. The strain reported (ε) was determined by the initial (L_0) and final (L) lengths of the crossheads in the following manner: $\varepsilon = (L - L_0)/L_0$. Force per width calculations were determined by the nominal force divided by the width of the tested sample (refer to Figure S12, Supporting Information, for lap-shear geometry). Adhesion strength was defined as the strength of the lap-shear sample immediately before the interface of the two adhered surfaces begins to separate.

Determination of Fracture Energy: Pure-shear tension test was applied to measure the fracture energy of the gel.[41] As indicated by Figure S10 (Supporting Information), the authors separately stretched two identical samples with the same thickness T_0, width W_0, and initial gage length L_0, where $W_0 >> L_0 >> T_0$. One sample was notched with a crack length of ≈0.5 W_0 and the other was unnotched. The notched sample was stretched to a critical distance L_c until crack starts to propagate while the unnotched sample was stretched to measure force–displacement curve. The fracture energy of the gel can be calculated by $\Gamma = \int_{L_0}^{L_c} F\,dl/W_0T_0$.

Digital Image Correlation: As is illustrated by Figure S10 (Supporting Information), digital image correlation was a noncontact optical technique that allows full-field strain measurement on a hydrogel surface under deformation.[42,43] Random speckle pattern was generated on the surface of a sample by spray painting. Images of speckle patterns at both reference state and deformed state were recorded by a standard video camera during the process of the deformation. Both images were transformed to gray matrices. To track the surface displacements of deforming materials, a mathematically well-defined correlated function was applied to match digitalized images before deformation and after deformation[44]

$$r(x,y) = 1 - \frac{\sum A(x,y)B(x^*,y^*)}{\left(\sum A(x,y)^2 * \sum B(x^*,y^*)^2\right)^{1/2}} \quad (1)$$

where $A(x, y)$ is the gray level at the location of (x, y) at reference state and $B(x^*, y^*)$ represents the gray level at the location of (x^*, y^*) at deformed state. The relation between (x^*, y^*) and (x, y) can be related as

$$\begin{cases} x^* = x + u + \dfrac{\partial u}{\partial x}\Delta x + \dfrac{\partial u}{\partial y}\Delta y \\ y^* = y + v + \dfrac{\partial v}{\partial x}\Delta x + \dfrac{\partial v}{\partial y}\Delta y \end{cases} \quad (2)$$

where u and v respectively represent the displacements in the direction of x and y. The displacements can be determined by minimizing the correlated function $r(x, y)$.

Supporting Information

Supporting Information is available from the Wiley Online Library or from the author.

Acknowledgements

M.A.G. and J.R.S. contributed equally to this work. The authors are grateful for support from the National Science Foundation Research Triangle Materials Research Science and Engineering Center (NSF MRSEC) (DMR-1121107), Pratt-Gardner Fellowship (J.R.S.), Medtronic Inc. Fellowship in BME (J.R.S.), and the NSF Graduate Research Fellowship Program (DGF1106401) (J.R.S.). X.Z. acknowledged the supports from the Office of Naval Research (ONR) (No. N00014-14-1-0528) and the NSF (No. CMMI-1253495).

Received: September 3, 2016
Revised: November 2, 2016
Published online:

[1] R. Langer, D. A. Tirrell, *Nature* **2004**, *428*, 487.
[2] J. R. McDaniel, J. A. MacKay, F. G. Quiroz, A. Chilkoti, *Biomacromolecules* **2010**, *11*, 944.
[3] N. Annabi, S. M. Mithieux, G. Camci-Unal, M. R. Dokmeci, A. S. Weiss, A. Khademhosseini, *Biochem. Eng. J.* **2013**, *77*, 110.
[4] J. Fang, A. Mehlich, N. Koga, J. Q. Huang, R. Koga, X. Y. Gao, C. G. Hu, C. Jin, M. Rief, J. Kast, D. Baker, H. B. Li, *Nat. Commun.* **2013**, *4*, 2974.
[5] M. J. Glassman, B. D. Olsen, *Soft Matter* **2013**, *9*, 6814.
[6] A. E. X. Brown, R. I. Litvinov, D. E. Discher, P. K. Purohit, J. W. Weisel, *Science* **2009**, *325*, 741.
[7] K. Nagapudi, W. T. Brinkman, J. Leisen, B. S. Thomas, E. R. Wright, C. Haller, X. Wu, R. P. Apkarian, V. P. Conticello, E. L. Chaikof, *Macromolecules* **2005**, *38*, 345.
[8] M. D. Golinska, M. K. Wlodarczyk-Biegun, M. W. T. Werten, M. A. C. Stuart, F. A. de Wolf, R. de Vries, *Biomacromolecules* **2014**, *15*, 699.
[9] B. J. Kim, D. X. Oh, S. Kim, J. H. Seo, D. S. Hwang, A. Masic, D. K. Han, H. J. Cha, *Biomacromolecules* **2014**, *15*, 1579.
[10] W. A. Petka, J. L. Harden, K. P. McGrath, D. Wirtz, D. A. Tirrell, *Science* **1998**, *281*, 389.
[11] S. Lv, D. M. Dudek, Y. Cao, M. M. Balamurali, J. Gosline, H. B. Li, *Nature* **2010**, *465*, 69.
[12] H. B. Li, W. A. Linke, A. F. Oberhauser, M. Carrion-Vazquez, J. G. Kerkviliet, H. Lu, P. E. Marszalek, J. M. Fernandez, *Nature* **2002**, *418*, 998.
[13] X. H. Zhao, *Soft Matter* **2014**, *10*, 672.
[14] C. Foo, J. S. Lee, W. Mulyasasmita, A. Parisi-Amon, S. C. Heilshorn, *Proc. Natl. Acad. Sci. USA* **2009**, *106*, 22067.
[15] C. M. Elvin, A. G. Carr, M. G. Huson, J. M. Maxwell, R. D. Pearson, T. Vuocolo, N. E. Liyou, D. C. C. Wong, D. J. Merritt, N. E. Dixon, *Nature* **2005**, *437*, 999.
[16] A. Valiaev, D. W. Lim, S. Schmidler, R. L. Clark, A. Chilkoti, S. Zauscher, *J. Am. Chem. Soc.* **2008**, *130*, 10939.
[17] D. C. Chow, M. R. Dreher, K. Trabbic-Carlson, A. Chilkoti, *Biotechnol. Prog.* **2006**, *22*, 638.
[18] W. Hassouneh, M. L. Nunalee, M. C. Shelton, A. Chilkoti, *Biomacromolecules* **2013**, *14*, 2347.
[19] M. K. McHale, L. A. Setton, A. Chilkoti, *Tissue Eng.* **2005**, *11*, 1768.
[20] C. Tallant, A. Marrero, F. X. Gomis-Ruth, *Biochim. Biophys. Acta, Mol. Cell Res.* **2010**, *1803*, 20.

[21] D. W. Lim, D. L. Nettles, L. A. Setton, A. Chilkoti, *Biomacromolecules* **2007**, *9*, 222.
[22] A. Ghoorchian, J. R. Simon, B. Bharti, W. Han, X. Zhao, A. Chilkoti, G. P. López, *Adv. Funct. Mater.* **2015**, *25*, 3122.
[23] P. Trumbo, A. A. Yates, S. Schlicker, M. Poos, *J. Am. Diet. Assoc.* **2001**, *101*, 294.
[24] D. E. Meyer, A. Chilkoti, *Nat. Biotechnol.* **1999**, *17*, 1112.
[25] L. J. Lapidus, P. J. Steinbach, W. A. Eaton, A. Szabo, J. Hofrichter, *J. Phys. Chem. B* **2002**, *106*, 11628.
[26] M. Rief, M. Gautel, F. Oesterhelt, J. M. Fernandez, H. E. Gaub, *Science* **1997**, *276*, 1109.
[27] S. Brahms, J. Brahms, G. Spach, A. Brack, *Proc. Natl. Acad. Sci. USA* **1977**, *74*, 3208.
[28] C. Chung, K. J. Lampe, S. C. Heilshorn, *Biomacromolecules* **2012**, *13*, 3912.
[29] Y. H. Cho, Y. J. Zhang, T. Christensen, L. B. Sagle, A. Chilkoti, P. S. Cremer, *J. Phys. Chem. B* **2008**, *112*, 13765.
[30] T. L. Sun, T. Kurokawa, S. Kuroda, A. Bin Ihsan, T. Akasaki, K. Sato, M. A. Haque, T. Nakajima, J. P. Gong, *Nat. Mater.* **2013**, *12*, 932.
[31] J. P. Gong, Y. Katsuyama, T. Kurokawa, Y. Osada, *Adv. Mater.* **2003**, *15*, 1155.
[32] R. E. Webber, C. Creton, H. R. Brown, J. P. Gong, *Macromolecules* **2007**, *40*, 2919.
[33] C.-Y. Hui, A. Jagota, S. J. Bennison, J. D. Londono, *Proc. R. Soc. London, Ser. A* **2003**, *459*, 1489.
[34] S. Rose, A. Prevoteau, P. Elziere, D. Hourdet, A. Marcellan, L. Leibler, *Nature* **2014**, *505*, 382.
[35] H. Yuk, T. Zhang, S. Lin, G. A. Parada, X. Zhao, *Nat. Mater.* **2016**, *15*, 190.
[36] H. Yuk, T. Zhang, G. A. Parada, X. Liu, X. Zhao, *Nat. Commun.* **2016**, *7*, 12028.
[37] D. E. Meyer, A. Chilkoti, *Nat. Biotechnol.* **1999**, *17*, 1112.
[38] G. Lee, K. Abdi, Y. Jiang, P. Michaely, V. Bennett, P. E. Marszalek, *Nature* **2006**, *440*, 246.
[39] E. L. Florin, M. Rief, H. Lehmann, M. Ludwig, C. Dornmair, V. T. Moy, H. E. Gaub, *Biosens. Bioelectron.* **1995**, *10*, 895.
[40] C. Chung, K. J. Lampe, S. C. Heilshorn, *Biomacromolecules* **2012**, *13*, 3912.
[41] R. S. Rivlin, A. G. Thomas, *J. Polym. Sci.* **1953**, *10*, 291.
[42] W. H. Peters, W. F. Ranson, *Opt. Eng.* **1982**, *21*, 213427.
[43] T. Zhang, S. Lin, H. Yuk, X. Zhao, *Extreme Mech. Lett.* **2015**, *4*, 1.
[44] H. A. Bruck, S. R. McNeill, M. A. Sutton, W. H. Peters III, *Exp. Mech.* **1989**, *29*, 261.